

# **Effect of Extrudate Swell, Nozzle Shape, and Convergence Zone on Fiber Orientation in Fused Deposition Modeling Nozzle Flow**

B. P. Heller\*, D. E. Smith\*, and D. A. Jack\*

\*Department of Mechanical Engineering, Baylor University, Waco, TX 76798

## **Abstract**

Recent advances for improving the mechanical properties of materials used in Fused Deposition Modeling (FDM) include the addition of carbon fibers to the filament feedstock. During processing, the flow field within the polymer melt orients the fiber suspension, which is important to quantify since fiber orientation influences mechanical and thermal properties. This paper presents a computational approach for evaluating polymer melt flow and fiber orientation within a FDM nozzle taking into consideration the converging flow in the nozzle, fluid expansion caused by extrudate swell, and nozzle exit shape. Finite elements are used to evaluate the Stokes flow in an axisymmetric nozzle and fiber orientation tensors are evaluated along streamlines within the flow using the Fast Exact Closure and Folgar-Tucker isotropic rotary diffusion. Fiber orientation is shown to increase in the shear-dominated flow through the nozzle, however, alignment is found to decrease in the expansion flow of the die swell.

## **Introduction**

Fused Deposition Modeling (FDM) is quickly becoming an industrially viable Additive Manufacturing (AM) technology. Intricate three dimensional parts can be created using low cost materials with little waste and low energy consumption. Another benefit to FDM is the ability to scale the technology to print very large parts with high dimensional accuracy. There still exist several issues with FDM that need to be addressed, such as warping, delamination, and unsatisfactory mechanical properties of typical FDM virgin polymers. The addition of carbon fibers to a virgin polymer was shown to significantly improve material integrity issues in FDM [1]. The addition of carbon fibers increases the strength and toughness of printed parts as well as reducing the CTE of the polymer fiber composite matrix. Unfortunately, little research has gone into the study of fiber orientation in the FDM process. Nixon, et al. [3] performed an initial study of the fiber orientation in three different FDM nozzle configurations (straight, converging, and diverging) with Moldflow (Moldflow Corporation, Framingham, MA) which uses the Advani Tucker [2] orientation tensor approach. The model produced by Nixon, et al. has the fiber filled polymer being injected into a large open mold and free surface open air boundary conditions are not considered. The fiber orientation in the polymer melt flow beyond the nozzle exit where the fluid boundary is partially formed by a free surface has yet to be studied for the FDM process. The extruded polymer melt will undergo extrudate swell at the nozzle exit which will affect the fiber orientation in the extruded bead; therefore, it is necessary to model this phenomena to produce an accurate model.

Fiber orientation in compression molding, injection molding, and extrusion has been studied for several decades and is well understood. The computationally efficient fiber orientation tensor approach introduced by Advani and Tucker [2] has become the standard

method for fiber orientation calculation. Fiber orientation software packages such as Moldflow (Moldflow Corporation, Framingham, MA) and Moldex3D (Core Tech Systems Co., Ltd., Chupei City, Taiwan) use the Advani and Tucker orientation tensor model to predict the fiber orientation in fiber filled molded parts. With respect to extrudate swell, studies have also been conducted on fiber orientation in rapid geometric changes (see [4] and [5]) which is beneficial to understanding how the fibers will react in the extrudate swell region. The inclusion of the free surface of the extrudate swell to the model will have an impact on the fiber orientation and therefore the material properties of the final printed part.

The swell of an extrudate at the exit of an extrusion die has also been studied and the phenomena is well understood. Extrudate swell will occur at the nozzle exit of the FDM nozzle and is therefore of interest to the current study. The extrudate swell has been modeled for Newtonian fluids by Georgiou, et al. [6] and Reddy and Tanner [7] using similar methods with slightly different parameters. The swell of the extrudate of a Newtonian fluid was calculated and observed to be approximately 13% from the nozzle exit diameter.

This paper presents a computational approach for computing fiber orientation in an axisymmetric FDM extrusion nozzle and within the polymer melt flow immediately after the polymer melt passes through the nozzle exit. The nozzle shape, convergence zone, and extrudate swell, and the effect of each on the fiber orientation state will be the focus in the current study. Fiber length is assumed to be sufficiently small to not clog the nozzle during printing. To model the fiber orientation we use the orientation tensor model of Advani-Tucker [2] and the Isotropic Rotary Diffusion model from Folgar and Tucker [8]. The Fast Exact Closure of Montgomery-Smith, et al. [9] is used to solve the orientation tensor closure problem. The fiber orientation is calculated for polymer melt flow through a 0.35 mm diameter FDM nozzle which is typical of many commercially available FDM devices, such as the Makerbot 2X (Makerbot Industries, LLC, Brooklyn, NY). The nozzle geometry is then changed in a parametric study to better understand the effect of nozzle geometry on fiber orientation.

### **Modeling Approach**

The cross section of a common FDM extrusion nozzle is used to create the polymer melt flow domain. An axisymmetric slice is taken from the cross section seen in Figure 1 and is used to define a finite element model of the flow domain in the COMSOL Multiphysics (Comsol, Inc., Burlington, MA) program as shown in Figure 2. Axial symmetry can be used as a computationally beneficial and physically accurate representation of a three dimensional flow. In the current study the analysis is restricted to axisymmetric flow in the nozzle and a region just outside of the nozzle exit. The boundary conditions used in the model appear in Figure 2.

It is assumed that the flow entering the nozzle is steady state laminar flow and thus the inlet velocity  $v_z^{inlet}$  in the  $z$  direction at  $z = 5.625 \text{ mm}$  is defined as

$$v_z^{inlet} = -v_{max} \left[ 1 - \left( \frac{r_{inlet}}{r_{max}} \right)^2 \right] \quad (1)$$

with  $v_x = v_y = 0$  at the inlet. In Equation (1),  $v_{max}$  is the maximum velocity at the inlet of the fluid domain,  $r_{inlet}$  is the radial location, and  $r_{max}$  is the maximum radius of the fluid domain at the inlet. For this study we use  $v_{max} = 4 \frac{mm}{s}$  and  $r_{max} = 0.875 \text{ mm}$ . This inlet velocity allows

for an average nozzle exit velocity of  $65 \frac{mm}{s}$  which is within the range of extrusion speeds for most desktop FDM printers.

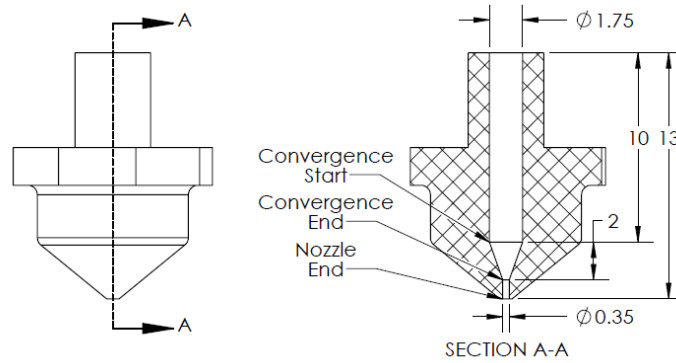


Figure 1. Cross Section of FDM Extrusion Nozzle, Dimensions are in millimeters (mm)

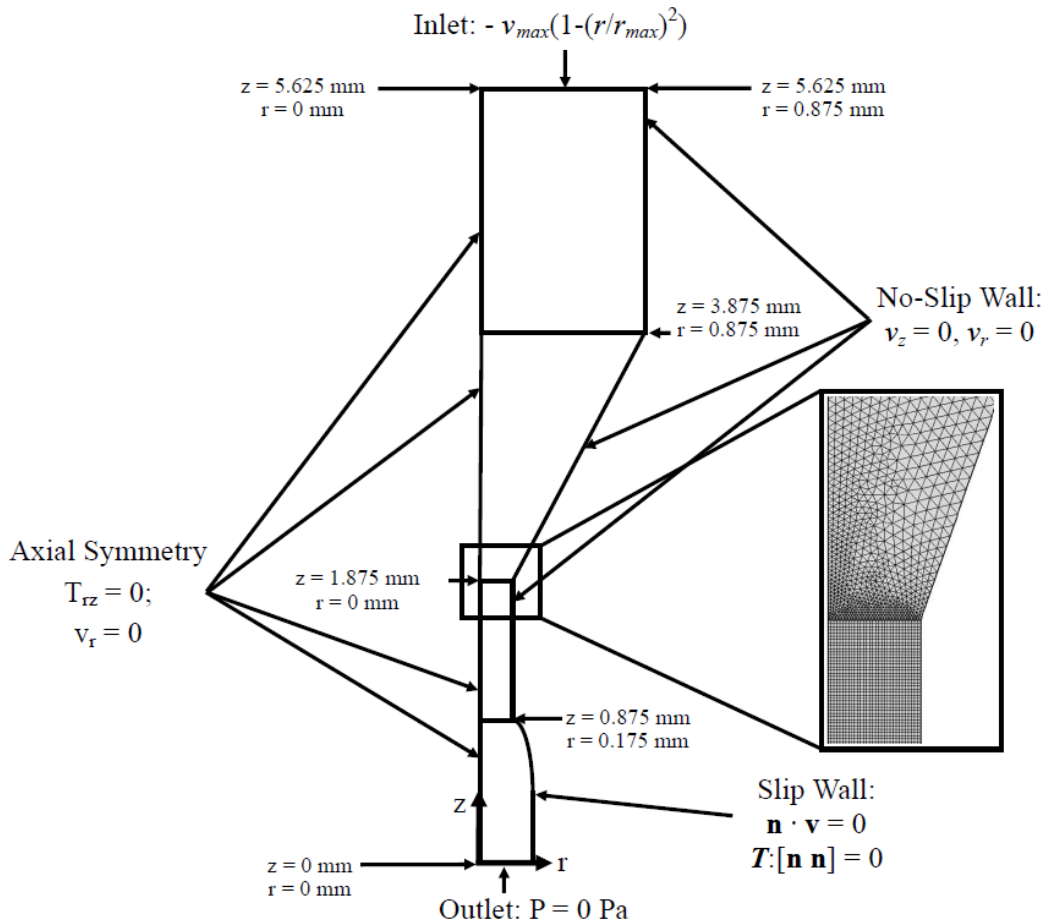


Figure 2. Boundary Conditions and Mesh for Nozzle Domain

The outlet at  $z = 0 \text{ mm}$  is defined as 0 Pa pressure. The exterior wall (right-hand side in Figure 2) of the fluid domain is defined as a no-slip wall boundary with  $v_z$  and  $v_r$  both equal to zero for  $z \geq 0.875 \text{ mm}$ . A slip wall condition is defined along the free surface defining the extrudate swell boundary for  $z < 0.875 \text{ mm}$ . A slip wall is defined by COMSOL Multiphysics as

$\mathbf{n} \cdot \mathbf{v} = 0$  where  $\mathbf{n}$  is the surface normal and  $\mathbf{v}$  is the velocity vector. The edge of the model at  $r = 0$  mm, an axisymmetric boundary condition is imposed.

The incompressible Newtonian fluid properties used in this simulation are density  $\rho = 1040$  kg/m<sup>3</sup> and dynamic viscosity of  $\mu = 350$  Pa·s. These values are chosen since they are for an ABS plastic, which is a common FDM printing material used in industry, at 230 degrees C and under a shear rate of 575 s<sup>-1</sup>, a value that is typical in the FDM nozzle flow domain. It is understood that ABS, is a shear-thinning non-Newtonian fluid. Assuming an isothermal Newtonian fluid simplifies the simulation process and is expected to be a good first step into the study of fiber orientation in deposition processes. Use of a Newtonian fluid also makes it possible to compare die swell results to known data from Georgiou [6] and Reddy and Tanner [7].

The finite element model is defined using the boundary conditions shown in Figure 2. A small sample of the mesh used is shown in Figure 2 as well. A mesh convergence study was performed during our preliminary studies to insure that a sufficiently fine mesh was employed so that the discretization would not affect the final results. The fluid flow problem is evaluated in Comsol Multiphysics using LiveLink which employs Matlab (The Mathworks, Inc., Natick, MA). The optimization approach described in Heller [?] which minimizes the combined shear and normal stress along the free surface is used here to compute the shape of the flow domain immediately outside of the nozzle exit. These results predicted a radial die swell of approximately 13% for straight tube flow which agrees well with values obtained by Georgiou, et al. [6] and Reddy and Tanner [7].

Fluid velocity and velocity gradients are calculated over the fluid domain, and fiber orientation through the nozzle is computed along streamlines within the flow domain. Ten streamlines appearing in Figures 4, 8, 9, and 11 (a) are computed at equally spaced locations across the nozzle outlet. At every point along the streamlines values of the velocity and velocity the gradients  $\left(u, w, \frac{du}{dr}, \frac{du}{dz}, \frac{u}{r}, \frac{dw}{dr}, \frac{dw}{dz}\right)$  are obtained for the evaluation of fiber orientation. Evaluation of fiber orientation is performed outside of COMSOL using Matlab. Fiber orientation is evaluated using the Advani and Tucker orientation tensor evolution equation given as [2]

$$\frac{DA}{Dt} = -\frac{1}{2}(\boldsymbol{\Omega} \cdot \mathbf{A} - \mathbf{A} \cdot \boldsymbol{\Omega}) + \frac{1}{2}\lambda(\boldsymbol{\Gamma} \cdot \mathbf{A} + \mathbf{A} \cdot \boldsymbol{\Gamma} - 2\mathbb{A}:\boldsymbol{\Gamma}) + \mathbf{D} \quad (2)$$

where the vorticity tensor is

$$\boldsymbol{\Omega} = [(\nabla\mathbf{v}) - (\nabla\mathbf{v})^T] \quad (3)$$

and the strain rate tensor is

$$\boldsymbol{\Gamma} = [(\nabla\mathbf{v}) + (\nabla\mathbf{v})^T] \quad (4)$$

In Equation (2),  $\mathbf{A}$  and  $\mathbb{A}$  are, respectively, the second and fourth-order fiber orientation tensors [2] and  $\lambda$  is a function of the fiber aspect ratio. The orientation diffusion term  $\mathbf{D}$  is defined from the Folgar-Tucker Isotropic Rotary Diffusion [8] model as

$$\mathbf{D}^{IRD} = 2C_I G(\mathbf{I} - 3\mathbf{A}) \quad (5)$$

where **IRD** indicates isotropic rotary diffusion. In this model,  $C_I$  is the empirically obtained interaction coefficient that is defined as  $C_I = 0.075$  for the present study, and  $\mathbf{I}$  is the identity tensor. The scalar magnitude of the rate of deformation  $G$  is defined as

$$G = \sqrt{\frac{1}{2} \mathbf{\Gamma} : \mathbf{\Gamma}} \quad (6)$$

Note that Equation (2) includes the fourth-order fiber orientation tensor which is required to compute the time rate of change of the second-order orientation tensor. The fourth-order orientation tensor's equation of motion has the sixth-order orientation tensor, and this continues for all even-ordered orientation tensors. In the present study we "close" this series using the Fast Exact Closure to approximate the fourth-order orientation tensor  $\mathbb{A}$ . When the Fast Exact Closure [6] is used, the equations of motion presented in Equation (2) for  $\mathbf{A}$  using Isotropic Rotary Diffusion are rewritten as [6]

$$\frac{D\mathbf{A}}{Dt} = -\frac{1}{2} \mathbb{C} [\mathbf{B} \cdot (\mathbf{\Omega} + \lambda \mathbf{\Gamma}) + (-\mathbf{\Omega} + \lambda \mathbf{\Gamma}) \cdot \mathbf{B}] + D_r (2\mathbf{I} - 6\mathbf{A}) \quad (7)$$

$$\frac{D\mathbf{B}}{Dt} = -\frac{1}{2} [\mathbf{B} \cdot (\mathbf{\Omega} + \lambda \mathbf{\Gamma}) + (-\mathbf{\Omega} + \lambda \mathbf{\Gamma}) \cdot \mathbf{B}] + D_r \mathbb{D} : (2\mathbf{I} - 6\mathbf{A}) \quad (8)$$

where  $\mathbb{C}$  and  $\mathbb{D}$  are fourth-order conversion tensors that are defined in Montgomery-Smith, et al., [6]. The tensor  $\mathbf{B}$  is a parameter of orientation defined similar to that of the orientation tensor  $\mathbf{A}$ . The fiber orientation equations (7) and (8) are solved to obtain the components of  $\mathbf{A}$  at points along the calculated streamlines. This approach provides a measure of fiber orientation at points throughout the FDM nozzle. In a related study we have investigated the pure shear steady state values of  $\mathbf{A}$  and  $\mathbf{B}$  for the given  $C_I$  and  $\lambda$  values to provide a more accurate inlet condition and to shorten the required length of the upstream region (cf. Heller [10]). The pure shear steady state inlet condition is used for all simulations given here and the associated plots.

In addition to calculating the fiber orientation in the standard nozzle appearing in Figure 1, a parametric study was performed to evaluate the effect of nozzle geometry on fiber orientation. Four parameters were selected to define different zones in the nozzle geometry as shown in Figure 3. Parameter A is the convergence zone length, B is the straight tube length, C is the amount of nozzle expansion, and D is the length of the nozzle expansion. To assess the effect of the nozzle geometry parameters on the fiber orientation, the average  $A_{33}$  was computed over a cross section of the free stream flow below the nozzle exit. The  $x_3$  direction is the longitudinal flow direction of the FDM nozzle, therefore, the  $A_{33}$  component is a measure of fiber alignment along the axial direction of the extrudate. The average value of the fiber orientation, which is defined as  $\bar{A}_{33}$ , at steady state after the nozzle exit is defined as

$$\bar{A}_{33} = \frac{2}{(r_{outer}^2 - r_{inner}^2)} I \quad (9)$$

where  $r_{outer}$  is the radial value of streamline 10,  $r_{inner}$  is the radial value of streamline 1, and  $I$  is the numerically integrated area under the curve defined by the  $A_{33}$  values at the ten discrete streamlines in the fluid domain. In equation (9)  $I$  is calculated using Simpson's 3/8 rule as

$$I = \frac{3}{8}h[F_1 + 3F_2 + 3F_3 + 2F_4 + 3F_5 + 3F_6 + 2F_7 + 3F_8 + 3F_9 + F_{10}] \quad (10)$$

In equation (10)  $F_i$  is defined as

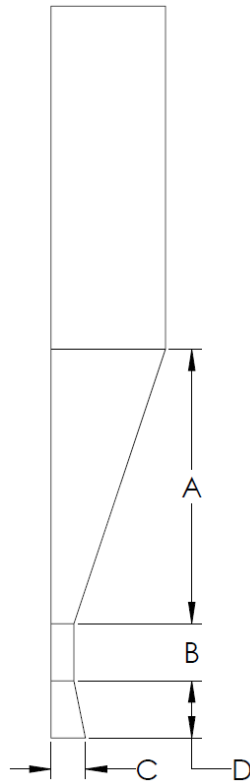
$$F_i = A_{33,i}r_i \text{ for } i = 1:10 \quad (11)$$

and  $h$  is defined as

$$h = \frac{r_{outer} - r_{inner}}{n} \quad (12)$$

In equation (12)  $n$  is the number of segments which is one less than the number of streamlines.

The average fiber alignment,  $\bar{A}_{33}$ , is calculated for fiber orientations evaluated within each of nozzle geometry defined by the parameters appearing in Figure 3. The parametric study is performed in two steps: first, thirty-six possible individual combinations are run for parameters A and B, second, the minimum fiber alignment case for flows defined by values of A and B is then used for the computation of each of the 18 possible combinations of C and D. From the parametric study the maximum fiber alignment case for A and B, the minimum fiber alignment case for A and B, and the max expansion case for C and D are of the greatest interest and will be discussed further in the results section.



**A = 5, 7, 9, 11, 13, and 15 radii**

**B = 0.1, 2, 4, 6, 8, and 10 radii**

**C = 1.025, 1.05, 1.075, 1.1, 1.125, and 1.15 radii**

**D = 1, 2, and 3 radii**

Figure 3. Nozzle Geometry Parameters and Values

## Results

Figures 4-6 below illustrate the results of our fiber orientation calculations within the nozzle flow of a typical FDM nozzle including the die swell region calculated as described above. For this study the flow domain is extended 5 exit radii past the extrusion nozzle exit to capture the effects of the extrudate swell. In Figures 4 and 5, **CZS** represents the start of the convergence zone of the nozzle, **CZE** represents the end of the convergence zone, and **NE** represents the extrusion nozzle exit. The location of **CZS**, **CZE**, and **NE** are shown in **Error! Reference source not found.**

In Figure 4 (a), the geometry and streamlines are shown for the FDM nozzle. Figure 4 (b) shows the  $A_{33}$  component for the 10 streamlines evaluated in the fluid domain. Figure 4 (b) also shows a measure of fiber alignment through the length of the nozzle and over the width of the nozzle at the 10 discrete streamlines that are plotted. This result shows the different effects that the orientation state encounters throughout the entire fluid domain.

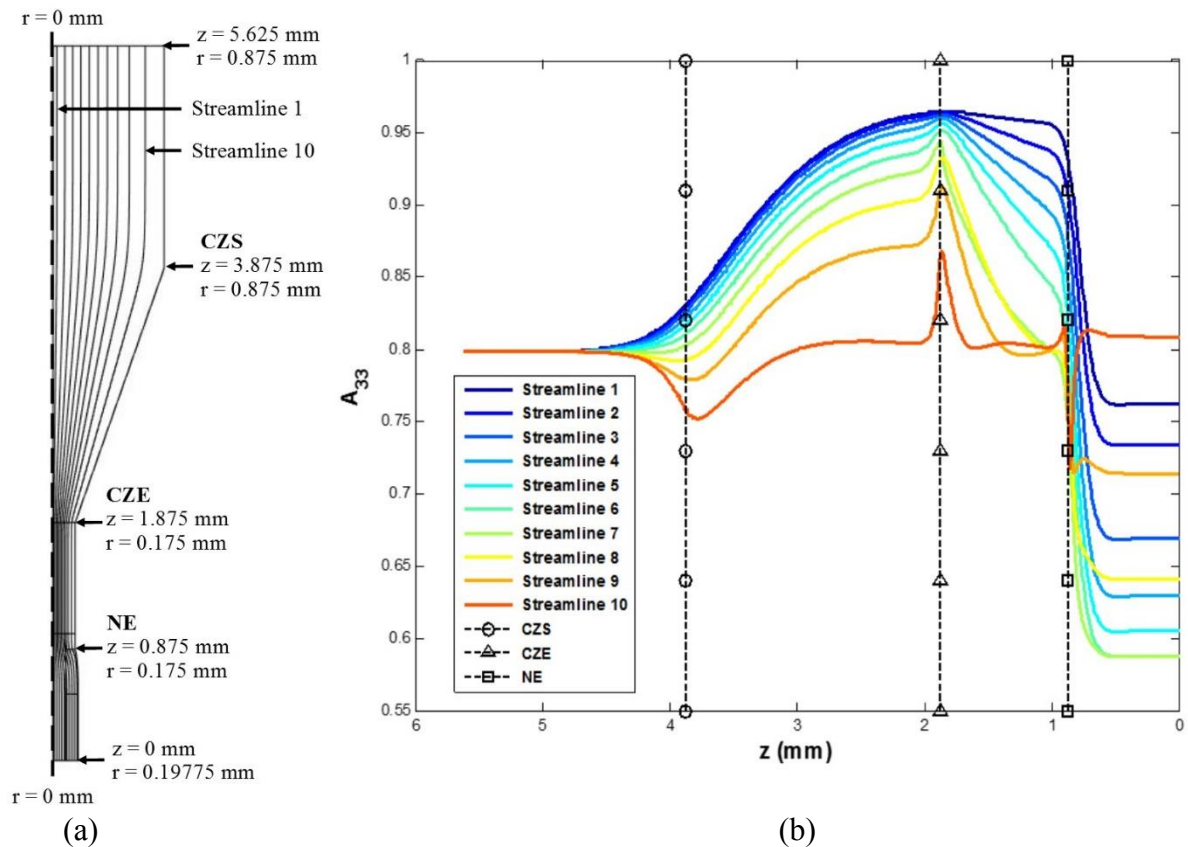


Figure 4. (a) Nozzle Geometry with Streamlines, (b)  $A_{33}$  along All Ten Streamlines

**Error! Reference source not found.** (b) shows the effects of the FDM nozzle geometry on the fiber orientation tensor  $A$ . **Error! Reference source not found.** (a) shows that the  $A_{33}$  component of the orientation tensor increases in the convergence zone which spans from **CZS** to **CZE** for streamlines 1-8.  $A_{33}$  reaches a value near unity, which represents a nearly uniaxial alignment in the  $z$ -direction. The maximum value of  $A_{33}$  at its peak is  $A_{33} = 0.9775$  along streamline 1. This increase in fiber orientation is due to elongation flow which is defined by an increase in

$\frac{\partial w}{\partial z}$  as seen in **Error! Reference source not found.** (d). The velocity gradient,  $\frac{\partial w}{\partial z}$  begins to increase before the convergence zone which causes a similar increase in the  $A_{33}$  component slightly before the convergence zone. Immediately after the end of the convergence zone, in the straight portion of the nozzle from **CZE** to **NE**, there is a decrease in the  $A_{33}$  component which can be related to the velocity gradients shown in **Error! Reference source not found.** (a & d). The velocity gradients  $\frac{\partial w}{\partial z}$  and  $\frac{\partial u}{\partial r}$  return to their zero in this region which causes a shear driven flow and results in the fiber orientation beginning to return to pure shear steady state orientation. After the nozzle exit, **NE**, there is a decrease in the  $A_{33}$  component of the fiber orientation which is due to the negative elongation component,  $\frac{\partial w}{\partial z}$ , and an expansion flow,  $\frac{\partial u}{\partial r}$ , shown in **Error! Reference source not found.** (a & d), both of which decrease the alignment in the  $A_{33}$  component.

In Figure 4 (b) it is seen that streamlines 9 and 10 undergo decreasing alignment over a short distance in the convergence zone of the nozzle. This is due to an increase in the expansion flow, as seen with  $\frac{\partial u}{\partial r}$  increasing faster the axial elongation gradient  $\frac{\partial w}{\partial z}$ . The magnitude of the elongation flow quickly surpasses expansion flow and the  $A_{33}$  component increases similar to streamlines 1-8 until **CZE**.

Figure (b) shows the  $A_{33}$  component of the orientation tensor throughout the fluid domain along all ten streamlines. It can be seen from Figure that the velocity gradient effects on the fiber orientation differ in magnitude depending on the spatial relation to the orientation changing flow. Because the magnitude of fluid velocity is greater at the center of the nozzle the elongation flow causes the fibers along streamline 1 to align more quickly in the axial direction than the fibers at streamline 10. This same effect causes the decrease of fiber alignment along the axis of flow at the nozzle exit to be greater than other streamlines further from the middle of the nozzle.

Figure 5 illustrates the velocity gradients along streamline 1. These velocity gradients are shown here since they directly influence changes in fiber orientation along streamline 1 throughout the nozzle. The velocities ( $u, w$ ) as well as the velocity gradient  $\left(\frac{u}{r}\right)$  along streamline 1 are not included in Figure 5 as these components have been found to have very little or no effect on the fiber orientation.



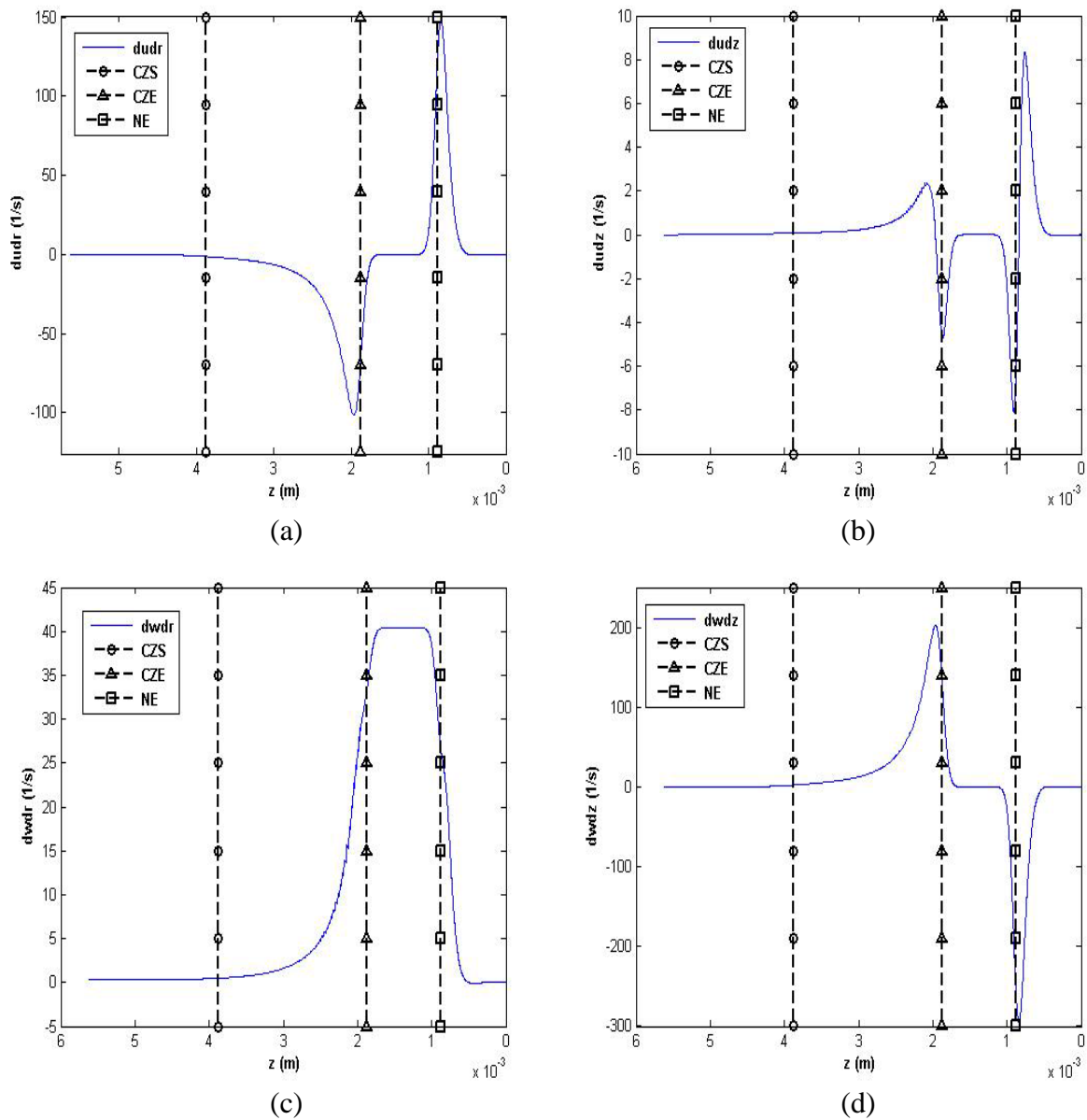


Figure 5. Velocity Gradients along Streamline 1

Figure 6 shows values of  $A_{33}$  at steady state at a cross section of the flow below the nozzle exit for the ten streamlines. Values of  $A_{33}$  that appear in Figure 6 provide a good indication of fiber alignment in the printed strand. With knowledge of this orientation, additional computations can be performed to determine the orientation pattern in an FDM printed part.

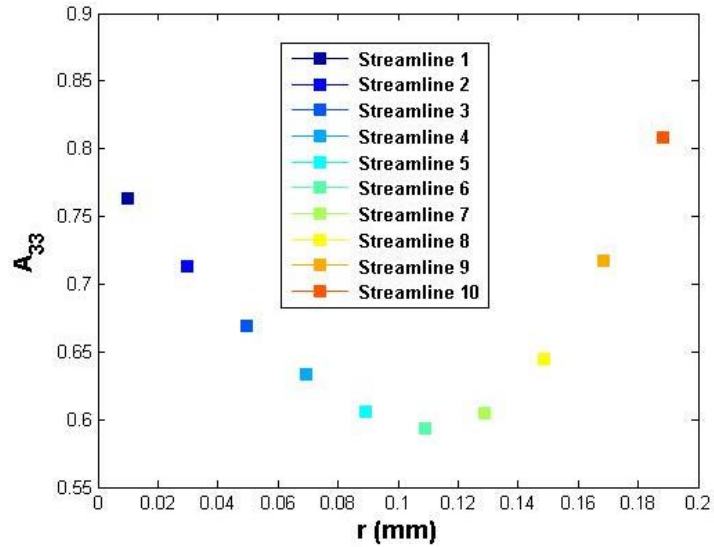


Figure 6.  $A_{33}$  Components for All 10 Streamlines

In Figure 6 it is seen that the fiber orientation is somewhat highly aligned for all values of radial position  $r$ , all showing greater than 0.55 alignment with the flow. Note that there is a high degree of alignment near the wall of the die at streamline 10 and high alignment at the center of the flow at streamline 1. There is also an obvious decline of orientation between the wall and the center of the flow. From this it can be deduced that the orientation of the fibers leaving the nozzle are highly aligned even considering the decrease in orientation right after the nozzle exit. This is due to the fact that the convergence zone has greatly increased the fiber alignment and that the effects of the extrudate swell cannot completely overcome the high fiber alignment.

Figure 7 shows the average fiber alignment in the direction of the flow,  $\bar{A}_{33}$ , for the thirty-six combinations of the A and B geometry parameters described above. Figure 7 illustrates the effect of changing certain portions of the nozzle geometry on the average fiber alignment. From this figure the maximum fiber alignment state (A = 5, B = 0.1) and the minimum fiber alignment state (A = 5, B = 10) are determined.

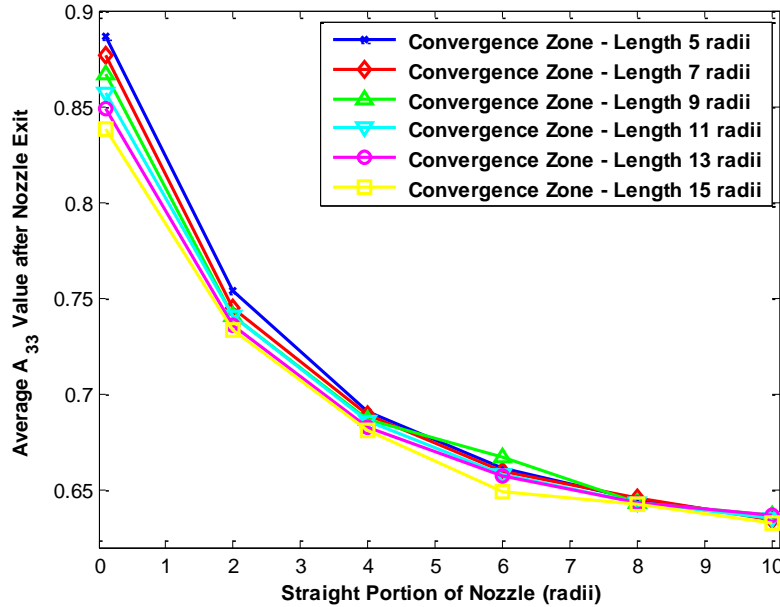


Figure 7. Average  $\bar{A}_{33}$  Value Downstream of the Nozzle Exit for Values of A and B

Figure 7 shows that parameter A, the length of the convergence zone, has very little effect on the amount of fiber alignment. The fiber alignment as measured by values of  $\bar{A}_{33}$  varies by only 0.1 over a range of 10 radii of nozzle length B. It is seen that parameter B, the length of the straight portion of the nozzle, has a much larger effect than parameter A. Parameter B decreases the fiber alignment substantially over 10 radii. This decrease in fiber alignment is due to pure shear flow in the straight portion which begins to return the orientation to the pure shear steady state orientation yielding a lower fiber alignment than that found immediately after the convergence zone ends.

In Figure 8 (a), the geometry and streamlines are shown for the maximum fiber alignment FDM nozzle configuration. Figure 8 (b) shows the  $A_{33}$  component for all 10 streamlines in the fluid domain. Figure 8 (b) also illustrates the amount of alignment as fluid travels through the length of the nozzle. This result shows the different effects that the orientation state encounters throughout the entire fluid domain.

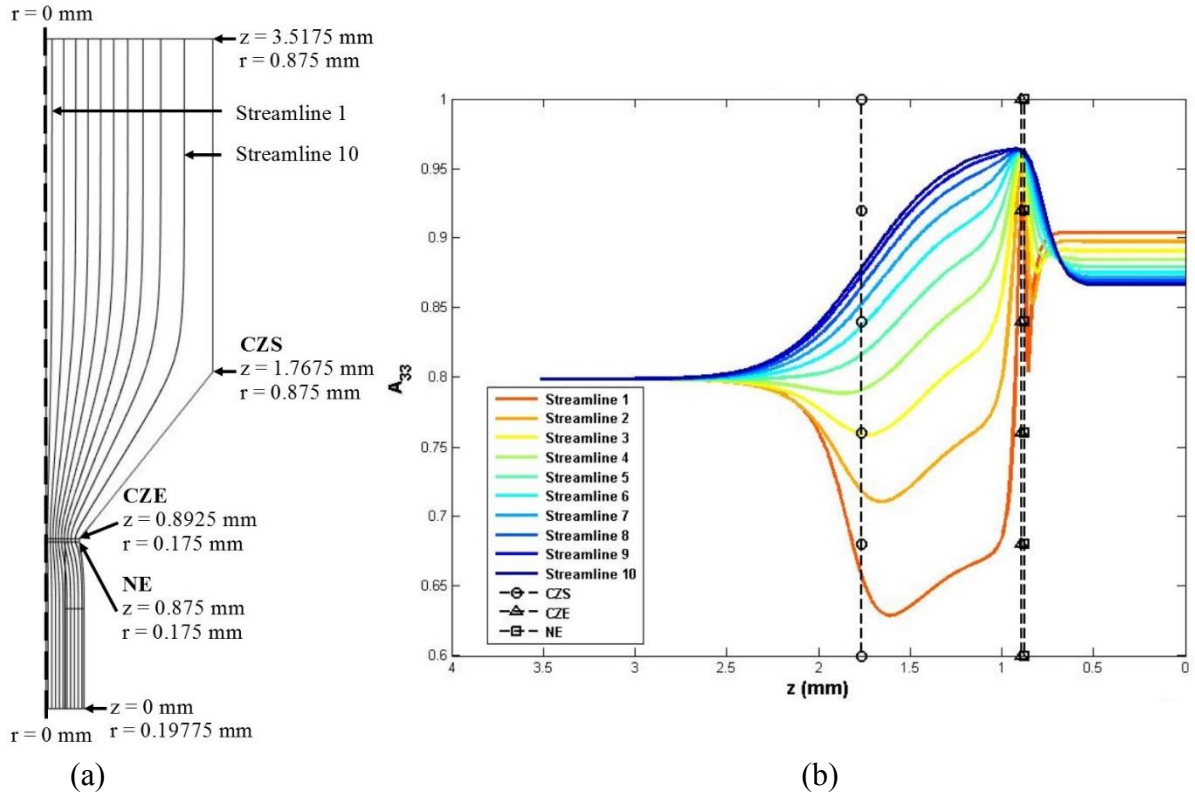


Figure 8. (a) Maximum Fiber Alignment State Nozzle Geometry with Streamlines, (b)  $A_{33}$  along All Ten Streamlines

Figure 8 (b) shows that streamlines 1-5 are very similar to those in Figure 4 (b) in that fiber alignment increases slightly before **CZS** and then continues to increase through to **CZE**. Streamlines 6-10 show a decrease in alignment from shortly before **CZS** to slightly after **CZS** then increase quickly to the **CZE**. The larger decrease in fiber alignment and the inclusion of more streamlines is due to the lower slope of the convergence zone wall than in the previous nozzle calculation. This allows for the magnitude of  $\frac{\partial u}{\partial r}$  to be greater than seen in previous calculations, and remain higher than  $\frac{\partial w}{\partial z}$  farther into the interior of the nozzle. The straight portion of the tube is only 0.1 radii, therefore there is almost no decrease in fiber alignment from **CZE** to **NE**. The expansion flow,  $\frac{\partial u}{\partial r}$ , and contraction flow,  $\frac{\partial w}{\partial z}$ , in the extrudate swell at the nozzle exit causes a decrease in the fiber alignment as seen before, but due to the initial fiber alignment being very high the overall fiber alignment remains high after the nozzle exit.

In Figure 9 (a), the geometry and streamlines are shown for the minimum fiber alignment FDM nozzle configuration. Figure 9 (b) shows the  $A_{33}$  component for 10 selected streamlines in the fluid domain. Figure 9 (b) also shows the amount of alignment throughout the length of the nozzle and over the width of the nozzle at the 10 discrete streamlines that are plotted. This result shows the different effects that the orientation state encounters throughout the entire fluid domain.

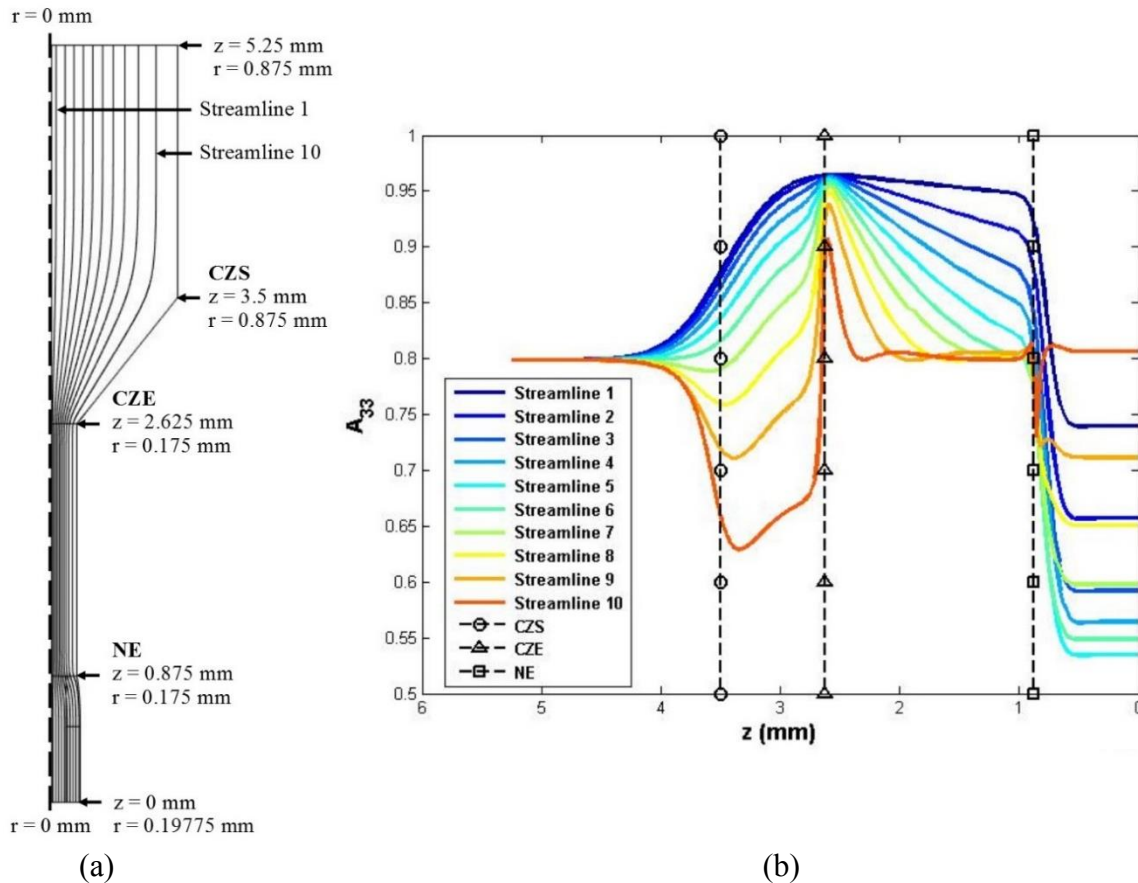


Figure 9. (a) Minimum Fiber Alignment State Nozzle Geometry with Streamlines, (b)  $A_{33}$  along All Ten Streamlines

In Figure 9 (b) streamlines 1-10 behave similar to those in Figure 8 (b) from inlet to **CZE** since the two simulations have the same initial geometry. From **CZE** to **NE** there is a decrease in fiber alignment for all streamlines. This is due to pure shear flow in the straight nozzle portion which decreases the fiber alignment towards the pure shear steady state value. After **NE** the expansion flow and contraction flow in the extrudate swell further decreases the fiber alignment.

Figure 10 shows the average fiber alignment in the direction of the flow,  $\bar{A}_{33}$ , for the eighteen possible combinations of the A, B, C, and D geometry parameters. From this figure, the maximum expansion case ( $A = 5$ ,  $B = 10$ ,  $C = 1.15$ , and  $D = 3$ ) is selected for further study to show the effects of an expanding nozzle near its exit.

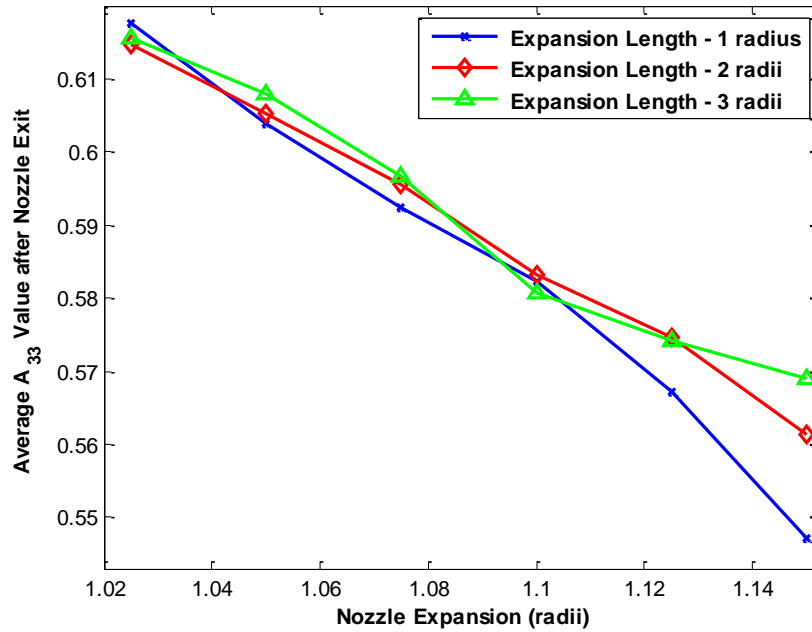


Figure 10. Average  $\bar{A}_{33}$  Value Downstream of the Nozzle Exit for Values of C and D, with A = 5, and B = 10

Figure 10 shows that parameter C, the amount of expansion of the nozzle, decreases the fiber alignment in the nozzle. Parameter D, the length of the nozzle expansion, is shown to have very little effect on the fiber alignment due to the tight bandwidth of the three expansion length lines. While parameter C does cause a decrease in fiber alignment it is a relatively small in comparison to parameter B. Larger values of expansion may cause a greater decrease in the fiber alignment, however, a maximum nozzle radial expansion of C = 1.15 is used here to ensure that the flow does not separate from the wall inside the nozzle.

In Figure 11 (a), the geometry and streamlines are shown for the maximum expansion FDM nozzle configuration. Figure 11 (b) shows the  $A_{33}$  component for all 10 calculated streamlines in the fluid domain. Figure 11 (b) also shows the degree of alignment throughout the length of the nozzle and over the width of the nozzle at the 10 discrete streamlines that are plotted. This result shows the different effects that the orientation state encounters throughout the entire fluid domain. In this figure, **STE** defines the Straight Tube Exit of the nozzle. Due to the expansion zone the end of the straight tube is no longer the nozzle exit, **NE**.

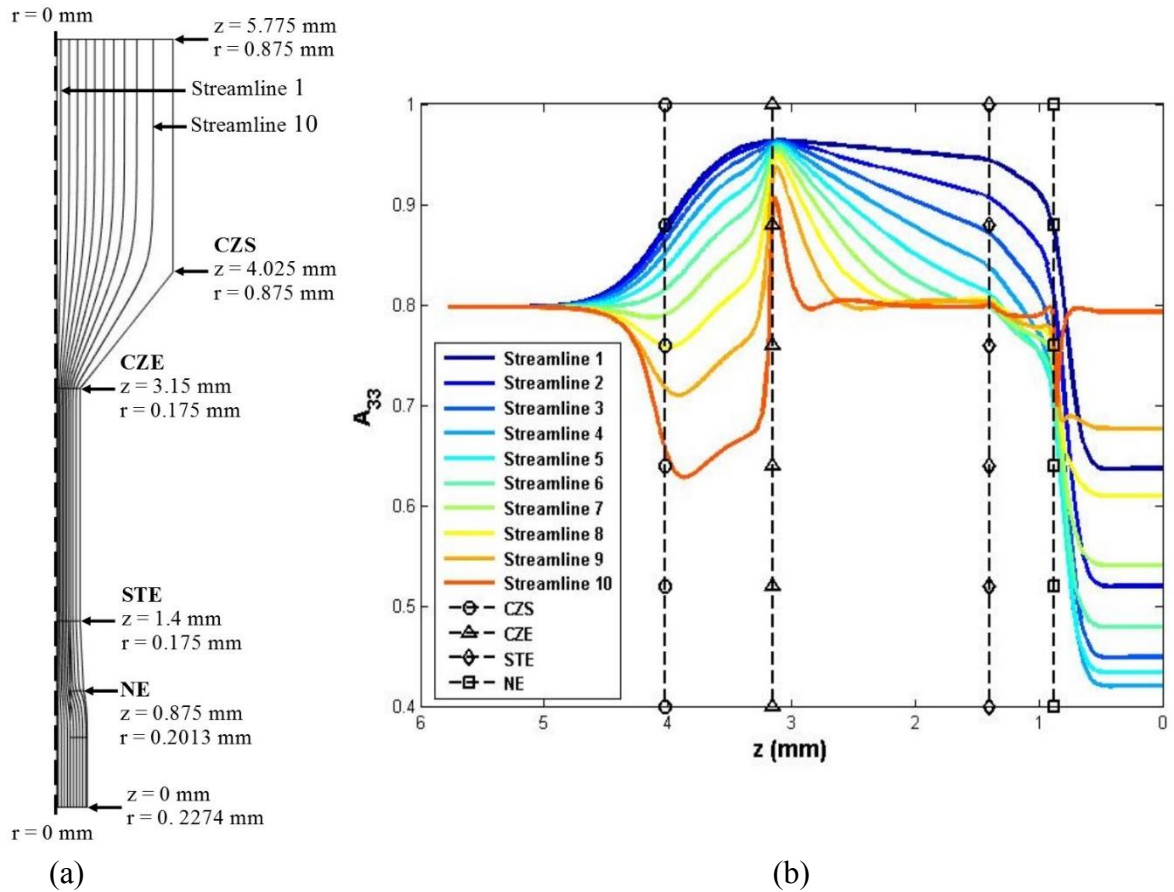


Figure 11. (a) Maximum Expansion Fiber Alignment State Nozzle Geometry with Streamlines, (b)  $A_{33}$  along All Ten Streamlines

Fiber orientation along streamlines 1-10 in Figure 11 (b) show trends similar to those in Figure 9 (b) from inlet to NE due to similarities in nozzle geometry. From STE to NE a decrease in fiber alignment is seen for all streamlines. This is due to expansion flow in the nozzle expansion zone which decreases fiber alignment. After NE there is a further decrease in fiber alignment due to expansion flow and contraction flow in the extrudate swell region. This is an important finding due to the fact that most FDM nozzles are in very close proximity to the printing platform. With this result the fiber orientation can be changed upstream from the nozzle exit before being deposited on the printing platform.

### Conclusions

It is shown in this study that the convergence zone and extrudate swell have a large impact on the fiber orientation state for short fiber suspension in the polymer melt during FDM deposition. The effect of the extrudate swell free surface on the fiber orientation was seen to be substantial. Since the extrudate swell is the last source of major fiber orientation change in the polymer melt it has a significant effect on the final orientation of the fiber suspension which defines the material properties of the finished part.

The parametric studies were run to further explore and quantify the effect of nozzle geometry on the resulting fiber alignment state. It was seen that a change in the nozzle convergence length (Parameter A) and the nozzle expansion length (Parameter D) had very little effect on the fiber alignment in the nozzle flow. The fiber alignment was seen to undergo more substantial decreases by changing the straight tube portion (Parameter B) and the amount of nozzle expansion (Parameter C). This result allows for the augmentation of nozzle geometry to provide a preferred fiber alignment state in the printed part.

This study uses the orientation tensor approach to fiber orientation in a viscous creeping flow. It is understood that the use of the Folgar-Tucker Isotropic Rotary Diffusion [5] function over-defines the rate of alignment of fibers in the transient solution, therefore in the future studies will be run using other well-known fiber orientation models to more exactly model the orientation throughout the extrusion nozzle. Also the addition of an average fiber orientation state across the entire strand of extruded polymer melt will be of interest for future studies. The current study does offer some interesting and respectively accurate information into the effects that the convergence zone of an FDM extrusion nozzle and the extrudate swell after the nozzle exit has on the fiber orientation of chopped fibers in extruded FDM parts. The knowledge of final orientation states of fibers in the polymer melt have great significance in the calculation of mechanical properties for the final FDM printed part. Using this tool designers can perfect the printing properties for FDM printing and create optimally designed parts that are viable for industrial uses

### **Future Work**

Many assumptions were made in this study that will affect the fiber orientation. In future studies the use of a Non-Newtonian fluid would be more accurate for the polymers that are used in FDM printing. Also, the current research calculates the problem for an isothermal fluid flow which would need to be changed to properly define true printing conditions. Another factor that would affect the fiber orientation which needs to be considered is fully coupled fiber orientation calculation. The orientation of the fibers changes the local viscosity, and therefore would affect the velocity gradients in the fluid flow and the resulting fiber orientation state. Three dimensional finite element modeling

### **References**

- [1] Love, L. J., Kunc, V., Rios, O., Duty, C. E., Elliot, A. M., The Importance of Carbon Fiber to Polymer Additive Manufacturing, *Journal of Materials Research, suppl. Focus Issue: The Materials Science of Additive Manufacturing*, **29**(17):1893-1898, 2014.
- [2] Advani, S., Tucker III, C., 1987. "The Use of Tensors to Describe and Predict Fiber Orientation in Short Fiber Composites". *Journal of Rheology*, Vol. 31
- [3] Nixon et. al., Three Parameter Analysis of Fiber Orientation in Fused Deposition Modeling Geometries. *SPE ANTEC 2014 – Proceedings of the Society of Plastics Engineers Annual National Technical Conference and Exhibition*, April 2014
- [4] VerWeyst, B.E., Tucker, C.L., Fiber Suspensions in Complex Geometries: Flow-Orientation Coupling. *The Canadian Journal of Chemical Engineering*, **80**:1093–1106, 2002.
- [5] Baloch, A., Webster, M.F., A Computer Simulation of Complex Flows of Fibre Suspensions, *Computers & Fluids*, **24**:135-151, 1995.
- [6] Georgiou, G.C., The Compressible Newtonian Extrudate Swell Problem, *International Journal For Numerical Methods in Fluids*, **20**:255-261, 1995



- [7] Reddy, K.R., Tanner, R.I., Finite Element Solution of Viscous Jet Flows with Surface Tension, *Journal of Computers and Fluids*, **6**:83-91, 1978.
- [8] Folgar, F., Tucker, C.L., "Orientatrimon Behavior of Fibers in Concentrated Suspensions" *Journal of Reinforced Plastics and Composites*, **30**:1-60, 1984
- [9] Montgomery-Smith, J. N., 2006. "The Fast Exact Closure for Jeffery's Equation with Diffusion", *Composites Part A, Applied Science and Manufacturing*, 43(2012), pp. 1959-1970
- [10] Heller, B., *Effects of Nozzle Geometry and Extrudate Swell on Fiber Orientation in Fused Deposition Modeling Nozzle Flow*, Master's Thesis, Baylor University, 2015.
- [11] COMSOL MULTIPHYSICS, The COMSOL Group, 1 New England Executive Park, Burlington Massachusetts 01803